



Abrupt shifts in the Indian monsoon during the Pliocene marked by high-resolution terrestrial records from the Yuanmou Basin in southwest China

Zhigang Chang, Jule Xiao ^{*}, Lianqing Lü, Haitao Yao

Key Laboratory of Cenozoic Geology and Environment, Institute of Geology and Geophysics, Chinese Academy of Sciences, Beijing 100029, China

ARTICLE INFO

Article history:

Received 19 January 2009

Received in revised form 29 June 2009

Accepted 12 August 2009

Keywords:

Yuanmou Basin

Fluvio-lacustrine sequence

Abrupt shifts

Indian monsoon

Pliocene

ABSTRACT

A 650-m-thick sequence of fluvio-lacustrine sediments from the Yuanmou Basin in southwest China was analyzed at 20-cm intervals for grain-size distribution to provide a high-resolution terrestrial record of Indian summer monsoon variations during the Pliocene. The concentrations of the clay and clay-plus-fine-silt fractions are inferred to reflect the water-level status of the lake basin related to the intensity of the Indian summer monsoon and high concentrations reflect high lake levels resulting from the intensified summer monsoon. The frequency of individual lacustrine mud beds is considered to reveal the frequency of the lakes developed in the basin associated with the variability of the Indian summer monsoon and an increased frequency of the lakes reveals an increased variability of the summer monsoon. The proxy data indicate that the Indian summer monsoon experienced two major shifts at 3.57 and 2.78 Ma and two secondary shifts at 3.09 and 2.39 Ma during the Pliocene. The summer monsoon displayed a general trend of gradual intensification during the period of 3.57–2.78 Ma, coeval with an accelerated uplift of the Tibetan Plateau, implying a close link between the monsoon intensification and the plateau uplift. At 2.78 Ma, the summer monsoon was markedly weakened, synchronous with the formation of extensive Northern Hemisphere ice sheets, denoting a quick response of the monsoon regime to the Northern Hemisphere glaciation. The variability of the summer monsoon decreased at 3.09 Ma and increased at 2.39 Ma, presumably suggesting that variations of the Indian monsoon would be modulated by the initiation and periodic fluctuations of ice-sheet covers in Northern Hemisphere high latitudes.

© 2009 Elsevier Ltd. All rights reserved.

1. Introduction

The Pliocene represents a period when Earth's boundary conditions underwent dramatic changes, such as the onset of Northern Hemisphere glaciation (Shackleton et al., 1995; Kleiven et al., 2002), the uplift of the Tibetan Plateau (An et al., 2001), and closure of Panamanian (Haug and Tiedemann, 1998) and Indonesian (Cane and Molnar, 2001) seaways. During this period, the global climate system experienced significant reorganizations in response to changes in Earth's boundary conditions (Zachos et al., 2001).

The Indian monsoon, an integral part of the global climate system, has been extensively studied through investigations of marine sediments from the Indian Ocean and the Arabian Sea (Clemens and Prell, 1990; Clemens et al., 1991; Kroon et al., 1991; deMenocal et al., 1991; Hovan and Rea, 1992; Chen et al., 1995; Gupta and Thomas, 2003; Gupta et al., 2004). During the Pliocene, however, the Indian monsoon variability and its possible causes have remained an enigma, because the resolution of the proxy records

from marine sediments is limited and few terrestrial records related to the Pliocene history of Indian monsoon variations are available.

In the present study, we provide a terrestrial sedimentary sequence from the Yuanmou Basin in southwest China. The sequence covers the entire Pliocene with an average temporal resolution of $\sim 45 \text{ yr cm}^{-1}$. The proxy records would greatly contribute to a better understanding of the process of Indian monsoon variations during the Pliocene and physical links between the Indian monsoon regime and other subcomponents of the global climate system.

2. Yuanmou Basin

The Yuanmou Basin (25°42'N, 101°53'E), a north–south stretched fault basin, lies 110 km northwest of Kunming, Yunnan Province, southwest China (Fig. 1). It has an area of 187 km² with a length of 30 km and a maximum width of 9 km (Li, 1993). The elevation of the basin ranges from 980 to 1400 m above sea level, while the surrounding mountains rise above the basin floor 1200–1400 m on the east and 200–400 m on the west. The Longchuan River flows through the basin from south to north toward its

^{*} Corresponding author. Address: Institute of Geology and Geophysics, Chinese Academy of Sciences, 19 Beitucheng West Road, Chaoyang District, Beijing 100029, China. Tel.: +86 10 8299 8380; fax: +86 10 6201 0846.

E-mail address: jlxiao@mail.iggcas.ac.cn (J.L. Xiao).

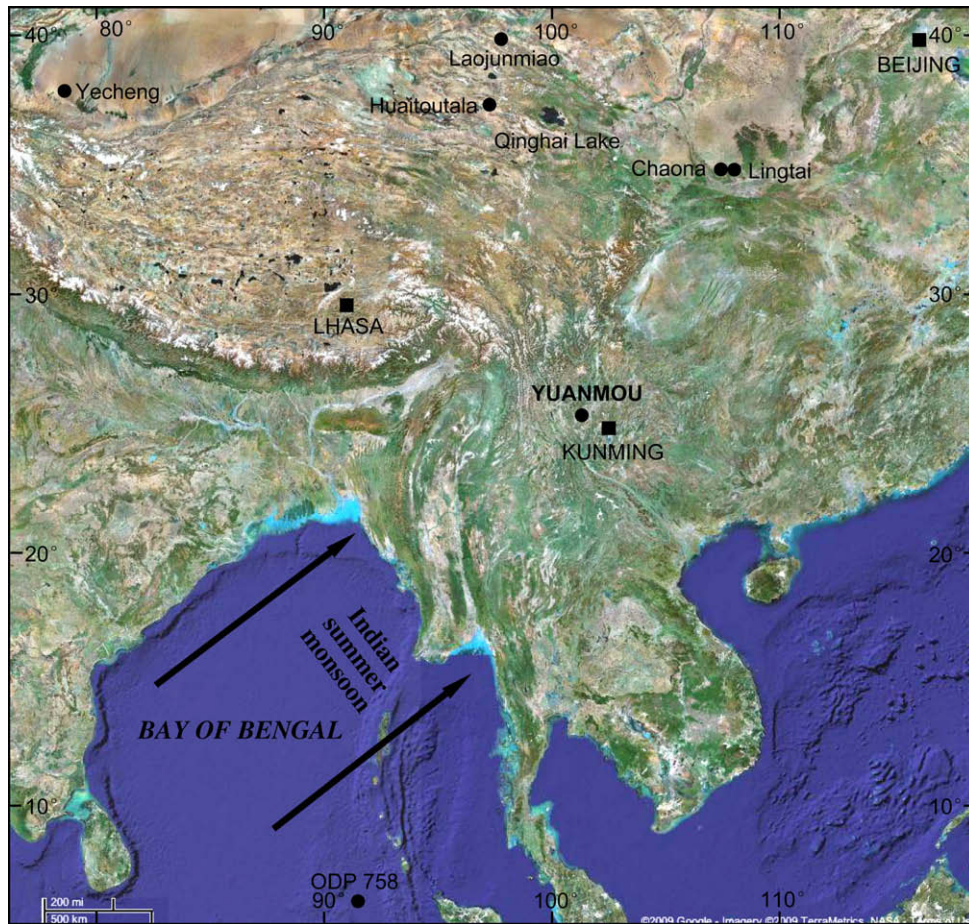


Fig. 1. Map (from <http://maps.google.com>) showing locations of the Yuanmou Basin and other terrestrial and marine records mentioned in the text. The bold arrows represent generalized wind directions of the Indian summer monsoon that brings rainfall from the tropical Indian Ocean to southwest China.

confluence with the Jinsha River, the uppermost reaches of the Yangtze River.

The basin is located in the south subtropical zone. The climate of the basin is controlled by the Indian monsoon in summer and by the southern stream of the westerly winds in winter (Li, 1993). Mean annual temperature is 21.9 °C, and mean annual precipitation is 614 mm with more than 80% of the annual precipitation falling in May–October. Mean annual evaporation reaches 3640 mm.

The Yuanmou Basin, one of the most representative Late Cenozoic sedimentary basins in China, was followed with interest as early as in 1920s when mammalian fossils were found from the basin (Colbert, 1940). During the subsequent decades, extensive investigations on the mammalian fauna were carried out, and fossils of *Equus* sp. of the latest Pliocene age (Bien, 1940) and *Enhydriodon* cf. *falconeri* of late Pliocene age (Chow, 1961) were discovered. In 1965, the discovery of two hominid incisors of *Homo erectus yuanmouensis* (Hu, 1973; Li et al., 1976; Qian et al., 1984) rejuvenated geologists' attention to the basin. Until now, however, most of the researches have been focused on the paleontology, sedimentology, lithostratigraphy and magnetostratigraphy (e.g., Qian and Zhou, 1991; Zhang et al., 1994; Urabe et al., 2001). Little attention was paid to the relation between the evolution of the lake basin and variations of the Indian monsoon.

3. Material and method

The sedimentary section selected for the present study extends east–west in the southern part of the Yuanmou Basin and passes by

Gantang and Maoyi villages (therefore designated GM section) (Figs. 2 and 3). It is exposed in erosional gullies and attains a thickness of 644 m with its base on the right bank of the Longchuan River.

3.1. Lithostratigraphy

The GM sedimentary sequence generally consist of brownish-red to greyish-brown fluvio-lacustrine mud and sands intercalated by frequent, greenish-grey and blackish-grey lacustrine mud beds and occasional, fluvial granule layers (Figs. 3 and 4). Lacustrine mud beds reach thicknesses of 0.4–5 m with the greenish-grey beds intervening from the base to the top of the section and the blackish-grey beds appearing only in the upper 271 m. The fluvio-lacustrine mud and sands, predominant deposits in the basin, generally display two sedimentary types, i.e., massive fluvial and laminated lacustrine mud and sands. Most of the granule layers are 40–80 cm thick with a few exceptions (1–4 m thick) at the depths around 170, 325, 430 and 472 m. The strata of the GM sequence tilt towards northeast to east and dip at 5–12°. Investigations in the field suggest that the GM section shows no signs of erosional hiatuses or faults.

3.2. Magnetostratigraphy

Paleomagnetic studies of the GM section were carried out to provide an age scale for the sedimentary sequence (Zhu et al., 2008). After orientated in situ with a magnetic compass, block

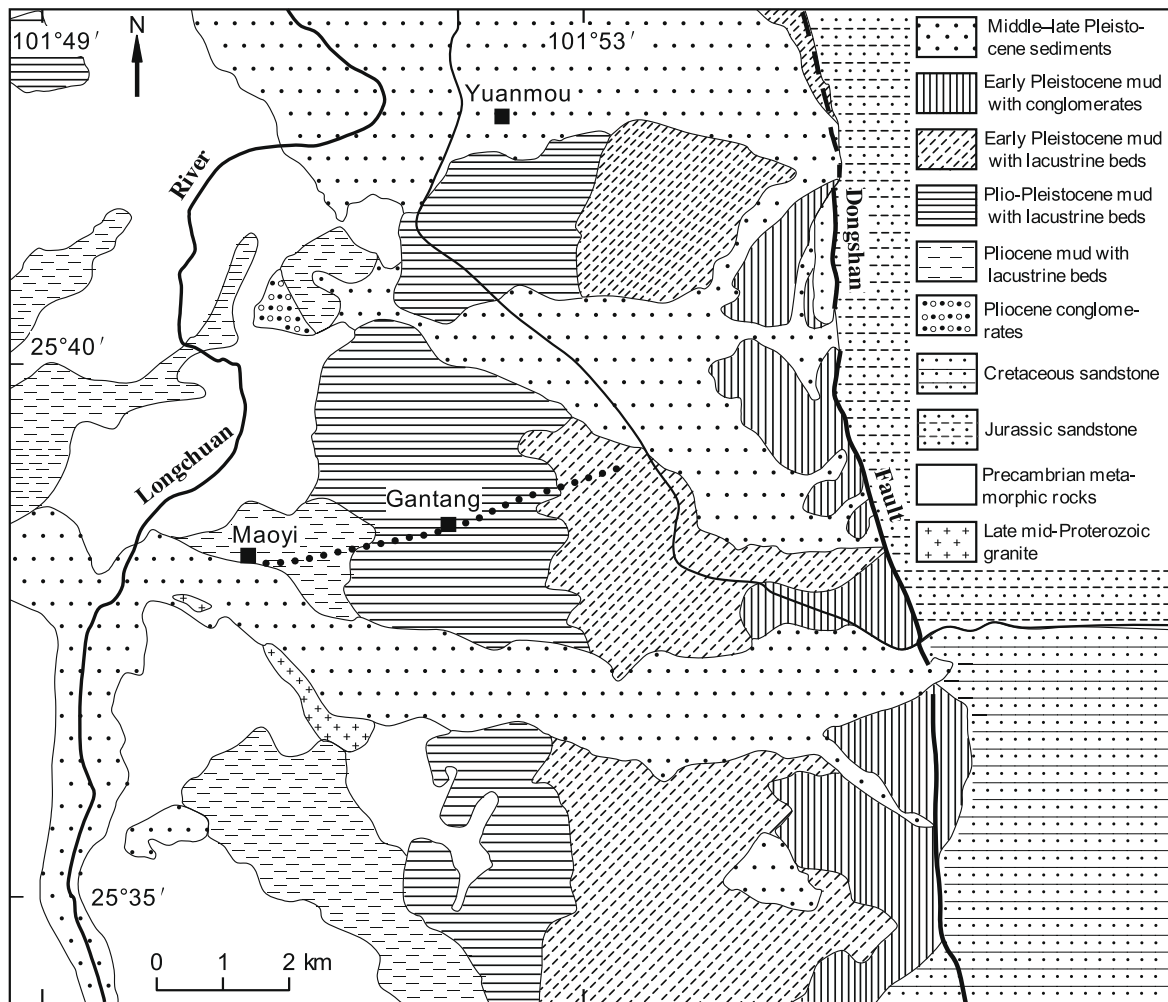


Fig. 2. Geological map of the Yuanmou Basin (modified from Jiang et al. (1989)). The dotted line passing by Gantang and Maoyi villages indicate the route of the sedimentary profile in the present study.

samples were taken at intervals of 20–50 cm, yielding 1208 samples for laboratory measurements. High-temperature magnetic susceptibilities were measured using a KLY-3s Kappabridge with a CS-3 high-temperature furnace in an argon atmosphere. All the samples were subjected to progressive thermal demagnetization up to 680 °C, and magnetic remanences were measured with a 2G, three-axis, cryogenic magnetometer housed in the field-free space. 579 samples (~48%) showed reliable characteristic remanent magnetization directions that were used to calculate the virtual geomagnetic pole (VGP) latitudes, resulting in the magnetic polarity sequence (Fig. 5).

Based on the Pliocene age of the mammalian fossils discovered from the GM section (Bien, 1940; Chow, 1961), the measured magnetic polarity sequence could be readily correlated to the geomagnetic polarity timescales (GPTS) (Berggren et al., 1995; Cande and Kent, 1995) (Fig. 5). The Matuyama/Gauss boundary lies at the depth of 141.80 m, whereas the Gauss/Gilbert boundary appears at the depth of 387.05 m. The short normal zone (32.30–38.05 m) above the Matuyama/Gauss boundary can be correlated to the Réunion subchron. Two reverse zones (258.10–272.55 and 332.80–353.95 m) within the Gauss normal chron represent Kaena and Mammoth subchrons. Three normal zones (443.80–459.05, 481.40–507.40 and 606.70–637.05 m) below the Gauss/Gilbert boundary correspond to Cochiti, Nunivak and Sidufjall subchrons.

3.3. Grain-size distribution

The GM section was sampled at 20-cm intervals continuously except the granule layers, yielding 3024 samples for analyses of grain-size distribution. About 200 mg of sediment from each air-dried, disaggregated sample was pretreated with 20 ml of 30% H₂O₂ to remove organic matter and then with 10 ml of 10% HCl with the sample solution boiled to remove carbonates. About 2000 ml of deionized water was added, and the sample solution was kept for 24 h to rinse acidic ions. The sample residue was dispersed with 10 ml of 0.05 M (NaPO₃)₆ on an ultrasonic vibrator for 10 min before grain-size analysis.

Grain-size distribution of the samples was determined with a Malvern Mastersizer 2000 laser grain-size analyzer. The Mastersizer works on the principle of the Mie theory that predicts the way light is scattered by spherical particles and deals with the way light passes through, or is absorbed by, the particle. Based on the Mie theory, assuming that measured particles are perfect spheres, the Mastersizer uses the volume of a particle to measure its size and calculate the diameter of an imaginary sphere that is equivalent in volume by the technique of “equivalent spheres”. The Mastersizer 2000 has a measurement range of 0.02–2000 μm in diameter and a grain-size resolution of 0.166φ in interval, thus yielding 100 pairs of grain-size data. It automatically outputs the median diameter and the percentages of the related size fractions of a sample with

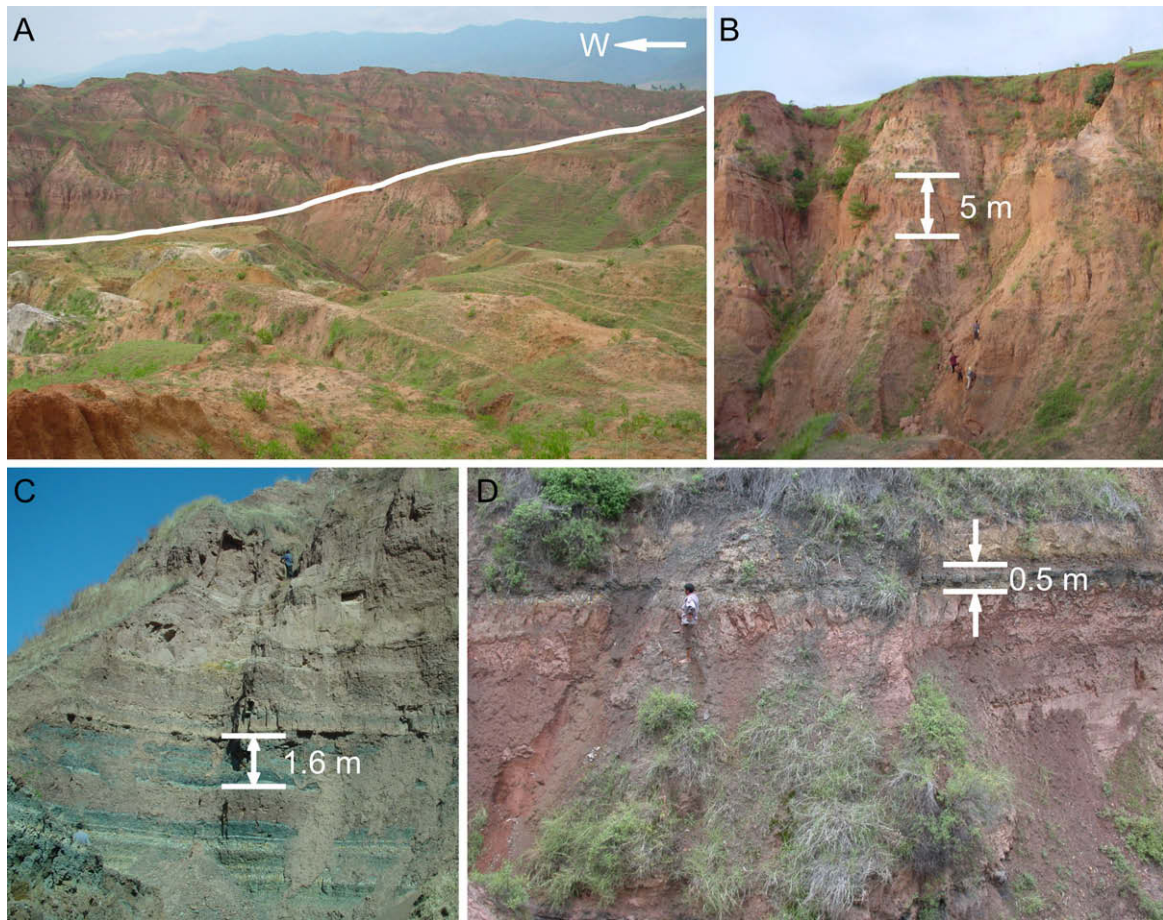


Fig. 3. Photographs of the outcrops showing (A) the erosional gully (white line) along which the sedimentary sections are exposed; (B) brownish-red to greyish-brown fluvio-lacustrine mud and sands at depth of 354.2–369.0 m; (C) greenish-grey lacustrine mud bed at depth of 185.0–201.5 m; (D) blackish-grey lacustrine mud bed at depth of 70.0–75.0 m. (For interpretation of the references to colour in this figure legend, the reader is referred to the web version of this article.)

a less than 1%. Data of the percentages of clay, silt and sand fractions from the GM sequence were plotted against depth in Fig. 5.

4. Proxies for the Indian summer monsoon

The nature and distribution of clastic deposits are mainly controlled by dynamic conditions of the transporting media (Inman, 1949; Folk and Ward, 1957; Tanner, 1964; Visser, 1969; Ashley, 1978; Håkanson and Jansson, 1983). Previous studies on grain-size distributions suggested that three types of clastic sediments exhibit different combinations of specific grain-size components. Fluvial deposits are composed mainly of two grain-size components, i.e., a saltation medium-sand component with dominant modal sizes of 200–400 μm and a suspension fine-silt component with dominant modal sizes of 10–15 μm (Middleton, 1976; Ashley, 1978; Bennett and Best, 1995). Grain-size components of eolian deposits depend on the nature of winds and transport distances (Pye, 1987; Sun et al., 2002). Typical loess deposits consist of a short-suspension, medium-to-coarse silt component with dominant modal sizes of 16–32 μm and a long-suspension clay-to-fine silt component with dominant modal sizes of 2–6 μm ; whereas desert sands mainly consist of a saltation component of fine-to-medium sands with dominant modal sizes of 100–200 μm and a suspension component of clay-to-fine silt with dominant modal sizes of 2–6 μm .

As compared with fluvial and eolian deposits, lake sediments display more complex, polymodal grain-size distributions (Visser, 1969; Middleton, 1976; Ashley, 1978; Sly, 1978), because the

hydraulic conditions in lakes are related to the water depth, shape, size and the surrounding relief (Sly, 1978, 1989a,b; Håkanson and Jansson, 1983). Fundamentally, there exists a relationship between clastic and hydraulic interactions, so that lake sediments can be separated into high and low hydraulic energy regimes (Sly, 1978, 1989a,b; Håkanson and Jansson, 1983). In general, the nearshore zone of lakes lies in higher energy environments than the offshore zone, and deposits of decreasing particle size towards the depocenter of lakes reflect decreasing hydraulic energy. The deposits of the offshore zone are dominated by clay and silty clay, whereas those of the nearshore zone consist of unconsolidated sands with low proportions of clay and silt (Sly, 1978, 1989a,b; Håkanson and Jansson, 1983).

The sediments of the GM sequence are mainly composed of lacustrine mud and fluvio-lacustrine mud and sands except occasional intercalations of fluvial granules (Figs. 4 and 5). Different grain-size components within individual grain-size distributions of the mud and sands would represent different sedimentary processes, thus denoting different hydrological conditions (Visser, 1969; Middleton, 1976; Ashley, 1978; Sly, 1978).

The hydrological condition of the Yuanmou Basin is largely controlled by the Indian summer monsoon that brings rainfall from the tropical Indian Ocean to southwest China. In general, the intensification of the summer monsoon would enhance the precipitation and inflow to the basin, leading to high stands of the lake developed in the basin. Therefore the formation and evolution of lakes in the Yuanmou Basin would have been closely related to variations of the Indian summer monsoon.

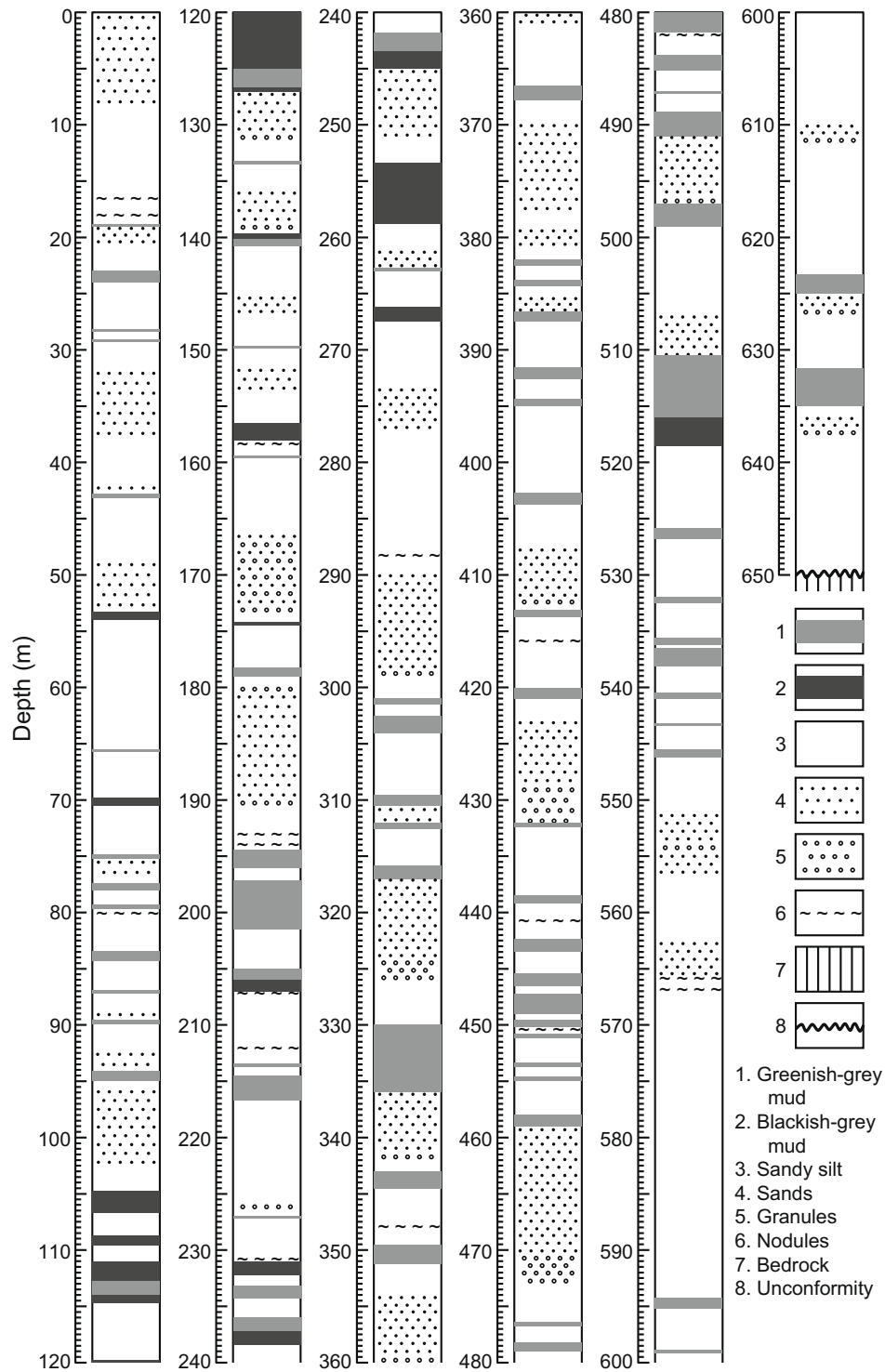


Fig. 4. Lithological column of the GM sedimentary sequence from the Yuanmou Basin, plotted against depth.

4.1. Concentrations of the clay and clay-plus-fine-silt fractions

In order to understand the evolution of sedimentary environments of the Yuanmou Basin, we compared grain-size distributions of lacustrine mud and fluvio-lacustrine mud and sands of the GM sequence with those of the surface sediments of a modern lake, Dali Lake in central-eastern Inner Mongolia, China (Fig. 6). The surface sediments were sampled at intervals of latitude 1' and longitude 1.5' and extracted in polyethylene tubes using a piston corer with

a length of 60 or 80 cm. Both the water-sediment interface and 2–3 mm of light coloured sediments are clearly discernible in the core tube, indicating that the uppermost part of the sediment core was deposited during the most recent years. The top 1 cm of the core sections was cut for samples of the surface sediments after siphoning the water from the core tube with a plastic pipe. Grain-size distributions of the surface samples suggested that the sediments of Dali Lake consist of homogeneous mud with increasing sand fractions toward the lakeshore (Xiao et al., 2009).

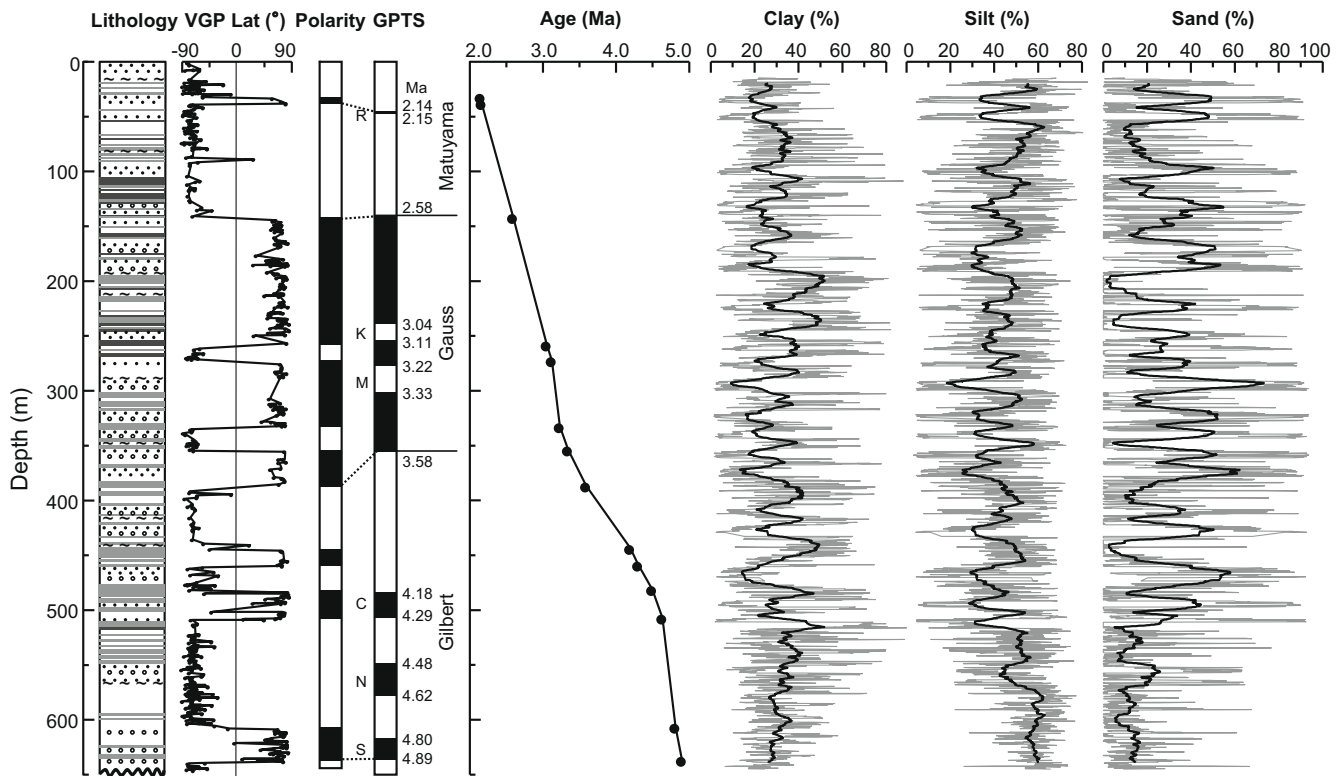


Fig. 5. Lithology, magnetostratigraphy, age–depth plots, and grain-size distribution (clay, %; silt, %; sand, %) records of the GM section from the Yuanmou Basin. For explanation of lithology, see Fig. 4. Latitudes of virtual geomagnetic pole (VGP) and the resultant polarity zones of the GM section (Zhu et al., 2008) are correlated with the standard polarity timescale (Berggren et al., 1995; Cande and Kent, 1995). R: Réunion, K: Kaena, M: Mammoth, C: Cochiti, N: Nunivak, and S: Sidufjall. Age–depth plots indicate age-control points of the GM section resulting from the paleomagnetic correlation (Zhu et al., 2008). The bold lines superimposed on the grain-size plots represent 51-point running means.

As shown in Fig. 6, the greenish-grey and blackish-grey lacustrine mud of the GM sequence shows grain-size distributions similar to the surface sediments of the offshore zone (clay- and fine-silt-dominated bimodal distribution) and the nearshore zone (fine-silt-dominated polymodal distribution) of Dali Lake, respectively. The fluvio-lacustrine mud and sands of the GM sequence display two distinct sedimentary types, i.e., fine-silt-dominated mud and sand- and coarse-silt-dominated sands, and the former resembles the lacustrine mud. In terms of the overall trend of decreases in the particle size of lake sediments from the nearshore to offshore zones, these observations led us to conclude that changes in the concentrations of the clay and clay-plus-fine-silt fractions of the GM sequence could reflect changes in the water-level status of the lakes controlled by the rainfalls of the Indian summer monsoon. High concentrations of both clay and clay-plus-fine-silt fractions would be closely related to high stands of the lake levels resulting from intensifications of the Indian summer monsoon.

4.2. Durations of the lacustrine mud beds

The most noticeable feature of the GM sedimentary sequence is the frequent intercalation of lacustrine mud beds. Greenish-grey beds intervene in the whole section and blackish-grey ones appear only in the upper 271 m (Figs. 4 and 5). There is no doubt that the lacustrine mud beds mark the occurrences of lakes in the Yuanmou Basin. Grain-size distributions of the lacustrine mud (Fig. 6) suggest that the greenish-grey beds stand for deep-water, large lakes in the basin and the blackish-grey ones for shallow-water, small lakes. In any case, the duration of the individual lacustrine bed would be linked with the lifetime of the lake developed in the basin. Long durations of the lacustrine beds could represent long

lifetimes of the lakes. Consequently judging from the whole sequence, frequent appearances of the lacustrine beds would be associated with frequent occurrences of the lakes in the basin. Because the formation and extinction of lakes in the Yuanmou Basin are closely related to the rainfalls brought by the Indian summer monsoon, the frequency of the lakes occurring in the basin would imply the variability of the summer monsoon. More frequent occurrences of the lakes would denote greater variability of the Indian summer monsoon.

The durations of all the lacustrine mud beds were plotted against age (Fig. 7) to understand changes in the frequency of lacustrine beds occurring at different times. The duration of individual lacustrine beds is the difference between ages of the bottom and the top that were derived by linear interpolation between paleomagnetic age-control points of the GM sequence.

4.3. Sedimentation rates

Paleomagnetic studies suggested that the GM sedimentary sequence covers the entire Pliocene (Zhu et al., 2008). The correlation between the measured magnetic polarity sequence and the geomagnetic polarity timescales (Berggren et al., 1995; Cande and Kent, 1995) yields 14 paleomagnetic ages for the GM sequence (Fig. 5). The sedimentation rates of all the polarity zones were derived by linear calculation between the paleomagnetic age-control points (Fig. 7).

Clastic materials in the sedimentary basin were derived from the catchment and transported by rivers and streams entering the basin (Håkanson and Jansson, 1983). In general, when the precipitation over the basin intensifies, the soil erosion in the catchment would be enhanced and the transport capacity of streams

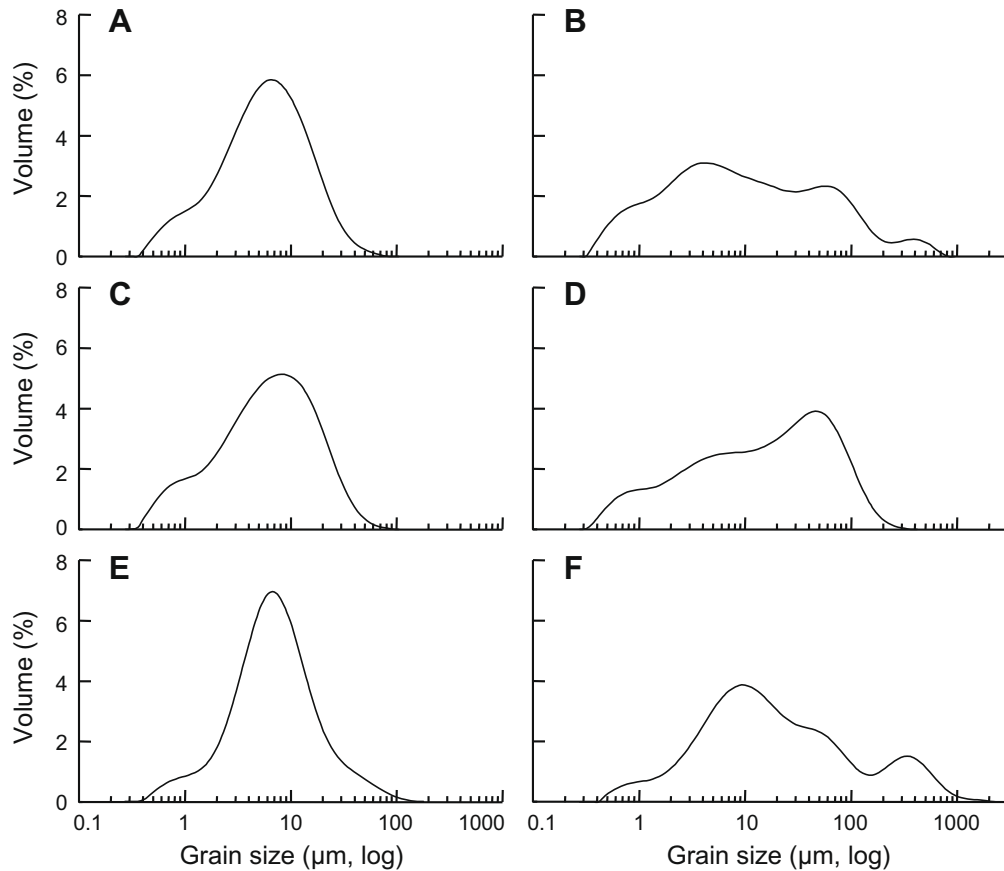


Fig. 6. Comparison of grain-size distributions of the Pliocene samples from the GM section in this study with those of the surface samples from Dali Lake in central-eastern Inner Mongolia, China. (A) Greenish-grey lacustrine mud of the GM sequence. (B) Blackish-grey lacustrine mud of the GM sequence. (C and D) Fluvio-lacustrine mud and sands of the GM sequence. (E) Mud from the offshore zone of Dali Lake. (F) Mud and sands from the nearshore zone of Dali Lake.

and rivers entering the basin would be increased, leading to an accelerated accumulation of clastic materials in the basin. Therefore increases in the sedimentation rate of the GM sequence might be associated with increases in the precipitation over the Yuanmou Basin and thus increases in the intensity of the Indian summer monsoon, provided regional tectonics was relatively stable.

5. Results and discussion

Concentrations of the clay and clay-plus-fine-silt fractions, durations of the greenish-grey and blackish-grey lacustrine mud beds and sedimentation rates of the GM sedimentary sequence were plotted against the paleomagnetic timescale (Fig. 7). Changes in the concentration of both the clay and clay-plus-fine-silt fractions are characterised by three stages during the Pliocene, i.e., fluctuations with declining amplitudes of the early stage, a general increasing trend with fluctuations of the middle stage, and fluctuations with similar amplitudes of the late stage (Fig. 7). The lower boundary between the early and middle stages was set at 3.57 Ma, the middle point between the below peaks of the fine fractions at 3.67 Ma and the above troughs at 3.47 Ma, whereas the upper one between the middle and late stages was set at 2.78 Ma, the middle point between the below peaks at 2.81 Ma and the above troughs at 2.75 Ma (Fig. 7).

As shown in Fig. 7, durations of the lacustrine mud beds of the GM sequence reflect two significant features. The blackish-grey lacustrine beds appeared in the sequence first at 3.09 Ma and the occurrence of the greenish-grey beds declined afterwards. And since 2.39 Ma, the durations of both the greenish-grey and

blackish-grey lacustrine beds became relatively shorter and the greenish-grey beds occurred more frequently.

The sedimentation rates of the GM sequence range from ~ 10 to 55 cm ka^{-1} with an average of $\sim 22 \text{ cm ka}^{-1}$ (Fig. 7). Judging from the overall trend of changes in the sedimentation rate, a significant increase from ~ 10 to 25 cm ka^{-1} occurred at 3.58 Ma. Additionally there are two intervals between 4.80 Ma (606.70 m) and 4.62 Ma (507.40 m) and between 3.22 Ma (332.80 m) and 3.11 Ma (272.55 m) showing exceptionally high sedimentation rates. During both intervals, the sediments mainly consist of sandy silt and clay (Figs. 4 and 5), presumably implying that the accelerated sedimentary filling might have resulted from the subsidence of the basin rather than the uplift of the surrounding mountains.

5.1. Gradual intensification of the Indian summer monsoon from 3.57 to 2.78 Ma

As shown in Fig. 7, both the clay and clay-plus-fine-silt fractions of the GM sequence displayed a general trend of increase in the concentrations during the period of 3.57–2.78 Ma. Meanwhile, this trend was accompanied by an increase in the sedimentation rate from ~ 10 to 25 cm ka^{-1} . These data suggest that the Indian summer monsoon was gradually intensified at the interval from 3.57 to 2.78 Ma.

Terrigenous mineral flux to the Indian Ocean initiated a dramatic increase 3.9 Ma ago, implying an enhanced process of weathering and erosion in the mountainous regions of the Tibetan Plateau since then (Hovan and Rea, 1992) (Fig. 7). Benthic foraminifer *U. proboscidea*, a productivity indicator species, began

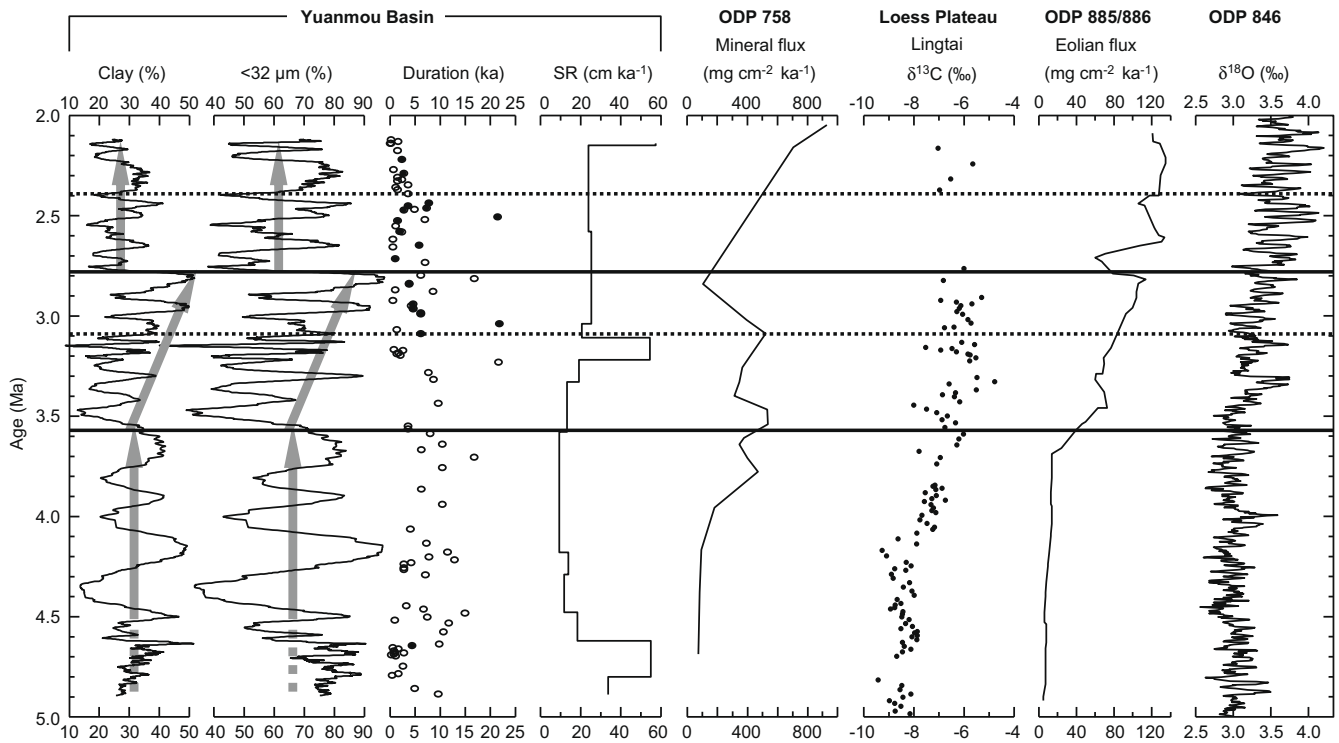


Fig. 7. Comparison of concentrations (%) of the clay and clay-plus-fine-silt (<32 μm) fractions, durations (ka) of the greenish-grey (circles) and blackish-grey (dots) lacustrine mud beds, and sedimentation rate (SR, cm ka^{-1}) of the GM sedimentary sequence of the Yuanmou Basin with mineral flux from ODP 758 in the eastern equatorial Indian Ocean (Hovan and Rea, 1992), pedogenic carbonate $\delta^{13}\text{C}$ of the red clay sequence at Lingtai in the Chinese Loess Plateau (Ding and Yang, 2000), eolian flux from ODP 885/886 in the North Pacific (Rea et al., 1998), and benthic foraminiferal $\delta^{18}\text{O}$ from ODP 846 in the eastern equatorial Pacific (Shackleton et al., 1995). The timescale of the GM sequence was derived by linear interpolation between paleomagnetic age-control points. Concentrations of the clay and clay-plus-fine-silt fractions are expressed as 51-point running means. Shaded arrows indicate the general trends of Indian summer monsoon variations during the periods before 3.57 Ma, between 3.57 and 2.78 Ma, and after 2.78 Ma, respectively. Solid and dashed lines mark abrupt shifts in the intensity and variability of the Indian summer monsoon during the Pliocene.

to thrive with high productivity in the northeastern Indian Ocean 4.2 Ma ago, denoting a significant increase in the intensity of the Indian summer monsoon at that time (Gupta and Thomas, 2003). Both records from the Indian Ocean provide support for our terrestrial-based inference that the Indian summer monsoon was intensified during the episode between 3.57 and 2.78 Ma.

The Indian monsoon is primarily driven by the thermal contrast between the Indian Ocean and the Asian continent (Webster, 1987). The rapid increase of the upwelling in the Arabian Sea at 8.5 Ma was interpreted as an indication of the origin or a strong intensification of the Indian monsoon system as a response to the uplifting of the Tibetan Plateau (Kroon et al., 1991). Numerical simulations suggested that the uplift of the Tibetan Plateau could heighten the land–sea thermal contrast and thus intensify the Indian summer monsoon (Hahn and Manabe, 1975; Prell and Kutzbach, 1992; Kutzbach et al., 1993). We therefore infer that the intensification of the Indian summer monsoon at 3.57–2.78 Ma marked by the terrestrial sedimentological records from the Yuanmou Basin would have been related to a phase of rapid uplift of the Tibetan Plateau.

The timing of uplift of the Tibetan Plateau has been hotly debated for several decades. Evidence from oxygen isotope values of carbonate rocks (Garzzone et al., 2000), activities of graben-bounding normal faults (Blisnuik et al., 2001), physiognomy of fossil leaves (Spicer et al., 2003), and oxygen isotope values of paleosol carbonates and lacustrine limestones (Rowley and Currie, 2006; DeCelles et al., 2007) suggest that the southern and central part of the Tibetan Plateau may have been uplifted 35–10 Ma ago. An alternative view is that the major uplifts occurred during the Pliocene and Pleistocene (Li, 1995). Detailed magnetostratigra-

phy of a fluvial sequence at Yecheng in the western Kunlun Mountains show a change from deposition on distal alluvial plains to proximal alluvial fans 4.5–3.5 Ma ago accompanied by an abrupt increase in the sedimentation rate at 3.6 Ma, indicating the main uplift of the northwestern Tibetan Plateau around that time (Zheng et al., 2000). The change from lacustrine mudstone–sandstone to alluvial conglomerates at the Laojunmiao section in the southern Jiuquan Basin (Fang et al., 2005) and a persistent rapid increase in the sedimentation rate of the Huaitoutala sequence in the eastern Qaidam Basin (Fang et al., 2007) occurred 3.6 Ma ago, and both were interpreted as the result of an accelerated uplift of the northeastern Tibetan Plateau at that time. Recent studies on the low-frequency magnetic susceptibility of the red clay sequence at Chaona on the Chinese Loess Plateau argue that the increase in sedimentation rate and grain size occurring around Tibet and in many other places 4.0 Ma ago would result from the rapid uplift of the Tibetan Plateau during the Pliocene rather than climate change, because the uplifted plateau could increase both the amplitude and the frequency of climatic fluctuations (Nie et al., 2008a,b). The view on the Pliocene uplift of the northern Tibet lends support to our inference that a phase of accelerated uplift of the Tibetan Plateau would have been the major causal factor in the intensification of the Indian summer monsoon at 3.57–2.78 Ma. The forcing mechanism lies in that the uplifted Tibetan Plateau receives more energy and the plateau surface becomes warmer in summer, leading to an increase in the thermal contrast between the Indian Ocean and the Asian continent, thus an intensified Indian summer monsoon.

Carbon isotopic compositions of pedogenic carbonates from the red clay sequence at Lingtai on the Chinese Loess Plateau exhibited a shift toward heavy values 4.1 Ma ago (Ding and Yang, 2000)

(Fig. 7). Eolian dust flux to the North Pacific showed a dramatic increase at 3.6 Ma (Rea et al., 1998) (Fig. 7). Both proxy records indicate that drying of the western China occurred at that time in response to the major phase of uplift of the Tibetan Plateau (Rea et al., 1998; Ding and Yang, 2000). These data further confirm the causal relation of intensification of the Indian summer monsoon to the uplift of the Tibetan Plateau during the period of 3.57–2.78 Ma. We infer that the accelerated uplift of the Tibetan Plateau during the Pliocene would be the causal factor both for the arid phase in the western China and for the wet phase in the study area, southwest China. The western China became dry because the uplifted plateau blocked the Indian summer monsoon and thus the monsoonal rainfall/moisture could not penetrate to the north of the plateau (Yeh and Gao, 1979), whereas the southwest China became wet because the Indian summer monsoon was strengthened and the southwest China could receive more monsoonal precipitations.

5.2. Marked weakening of the Indian summer monsoon at 2.78 Ma

An abrupt and large-scale decrease in the concentrations of clay and clay-plus-fine-silt fractions of the GM sequence occurred at 2.78 Ma, suggesting a marked decrease in the intensity of the Indian summer monsoon at that time (Fig. 7). This interpretation is directly supported by drastically decreased influxes of terrigenous materials to the Indian Ocean about 2.8 Ma ago (Hovan and Rea, 1992) (Fig. 7).

Pliocene high-resolution oxygen isotope record of benthic foraminifers from ODP Site 846 in the eastern Pacific reveals a significant shift toward heavy $\delta^{18}\text{O}$ values about 2.75 Ma ago (Shackleton et al., 1995) (Fig. 7). Records of ice-rafted detritus from ODP Sites 644 and 907 in the Nordic Seas and DSDP Sites 610 and 607 in the North Atlantic Ocean document that an ice-sheet development between the Greenland, Scandinavian and North America regions started around 2.72–2.75 Ma (Kleiven et al., 2002). The remarkable weakening of the Indian summer monsoon at 2.78 Ma almost coincides with the heavier shift in the $\delta^{18}\text{O}$ of benthic foraminifers and the formation of extensive Northern Hemisphere ice sheets, suggesting a teleconnection between the low-latitude monsoon system and the high-latitude glaciation. We infer that the decreased intensity of the Indian summer monsoon would have resulted from the intensification of the Northern Hemisphere glaciation. The Northern Hemisphere glaciation could enhance global cooling (Shackleton et al., 1995), resulting in an increased snow/ice cover on the uplifted Tibetan Plateau. This change could increase plateau surface albedo and decrease surface temperature in summer, giving rise to a reduced land–sea thermal contrast and thus a weakened Indian summer monsoon (Prell and Kutzbach, 1992).

5.3. Shifts in the Indian monsoon variability 3.09 and 2.39 Ma ago

The initial appearance of the blackish-grey lacustrine beds at 3.09 Ma accompanied with occasional occurrences of the greenish-grey beds may reflect a decreased variability of the Indian monsoon since then (Fig. 7). It is suggested that the first major pulse of ice-rafted detritus in the circum Atlantic region happened at 3.3 Ma and progressive increases in ice-rafted detritus took place from 3.0 Ma (Kleiven et al., 2002). The onset of large-scale glaciation in the circum Atlantic region was accompanied by a change to decreased variability of the Indian summer monsoon, implying a linkage between the initial glaciation in the Arctic region and the variability of the Indian summer monsoon. Although we are not certain of the exact mechanism, we speculate that the vegetation cover on the Tibetan Plateau might have played an active role in adjusting the monsoon variability during the period after the plateau already exceeded a threshold altitude but before

extensive Northern Hemisphere ice sheets appeared. The vegetation cover on the plateau would reduce plateau surface albedo and absorb more energy in the soil–vegetation–atmosphere coupled system, leading to a decreased seasonal temperature difference. The decreased seasonality might have strengthened the Indian summer monsoon and weakened the winter monsoon, resulting in decreased monsoon variability. This scenario is supported by a modelling study (Wang, 1999).

At 2.39 Ma, however, an increase in the frequency and a decrease in the duration of the lacustrine mud beds indicate a significant shift to greater variability of the Indian summer monsoon (Fig. 7). A detailed magnetic susceptibility record of eolian dust deposition to the Arabian Sea at ODP Sites 721 and 722 reveals a dramatic increase in variance at the 41-ka periodicity corresponding to orbital obliquity after 2.4 Ma (deMenocal et al., 1991). This shift to increased 41-ka power after 2.4 Ma was proposed to reflect the modulation of monsoon dust source area aridity by high-latitude ice-sheet cover that varied predominantly at this periodicity (deMenocal et al., 1991). The timing of the shift to increased variability of the Indian summer monsoon coincides with the inception of predominance of the 41-ka periodicity, presumably denoting that the Indian monsoon regime itself might have been modulated by periodic fluctuations in high-latitude ice-sheet cover since 2.39 Ma.

6. Conclusions

High-resolution terrestrial sedimentary records from the Yuanmou Basin in southwest China indicate that the Indian summer monsoon experienced two major shifts at 3.57 and 2.78 Ma and two secondary shifts at 3.09 and 2.39 Ma during the Pliocene. The summer monsoon was gradually intensified from 3.57 to 2.78 Ma and markedly weakened 2.78 Ma ago. The monsoon variability displayed a decrease at 3.09 Ma and an increase at 2.39 Ma. Variations of the Indian monsoon during the Pliocene would have been closely related both to the uplift of the Tibetan Plateau and to the high-latitude glaciations in the Northern Hemisphere.

Acknowledgments

We thank two anonymous reviewers for valuable comments and suggestions. We greatly appreciate the contributions by Rixiang Zhu, Yongxin Pan, Chenglong Deng and Feng Gao in the reconnaissance of the Yuanmou Basin. This study was financially supported by grants 2004CB720202 and NSFC 40599422.

References

- An, Z.S., Kutzbach, J.E., Prell, W.L., Porter, S.C., 2001. Evolution of Asian monsoons and phased uplift of the Himalaya–Tibetan Plateau since Late Miocene times. *Nature* 411, 62–66.
- Ashley, G.M., 1978. Interpretation of polymodal sediments. *Journal of Geology* 86, 411–421.
- Bennett, S.J., Best, J.L., 1995. Mean flow and turbulence structure over fixed, two-dimensional dunes: Implications for sediment transport and bed form stability. *Sedimentology* 42, 491–513.
- Berggren, W.A., Kent, D.V., Swisher III, C.C., Aubry, M.P., 1995. A revised Cenozoic geochronology and chronostratigraphy in time scales and global stratigraphic correlations: a unified temporal framework for a historical geology. In: Berggren, W.A., Kent, D.V., Aubry, M.P., Hardenbol, J. (Eds.), *Geochronology, Timescales, and Stratigraphic Correlation*, Spec. Publ. No. 54. Society of Economic Paleontologists and Mineralogists, Tulsa, pp. 129–212.
- Bien, M.N., 1940. Geology of the Yuanmo Basin, Yunnan. *Bulletin of the Geological Society of China* 20, 23–31.
- Blisnuik, P.M., Hacker, B.R., Glodny, J., Ratschbacher, L., Bi, S.W., Wu, Z.H., McWilliams, M.O., Calvert, A., 2001. Normal faulting in central Tibet since at least 13.5 Myr ago. *Nature* 412, 628–632.
- Cande, S.C., Kent, D.V., 1995. Revised calibration of the geomagnetic polarity timescale for the Late Cretaceous and Cenozoic. *Journal of Geophysical Research* 100, 6093–6095.

- Cane, M.A., Molnar, P., 2001. Closing of the Indonesian seaway as a precursor to east African aridification around 3–4 million years ago. *Nature* 411, 157–162.
- Chen, J.J., Farrell, J.W., Murray, D.W., Prell, W.L., 1995. Timescale and paleoceanographic implications of a 3.6 m.y. oxygen isotope record from the northeast Indian Ocean (Ocean Drilling Program site 758). *Paleoceanography* 10, 21–47.
- Chow, M.C., 1961. Occurrence of *Enhydriodon* at Yuanmo, Yunnan. *Vertebrata Palasiatica* 19, 164–167.
- Clemens, S.C., Prell, W.L., 1990. Late Pleistocene variability of Arabian Sea summer monsoon winds and continental aridity: eolian records from the lithogenic component of deep-sea sediments. *Paleoceanography* 5, 109–145.
- Clemens, S., Prell, W., Murray, D., Shimmield, G., Weedon, G., 1991. Forcing mechanisms of the Indian Ocean monsoon. *Nature* 353, 720–725.
- Colbert, E.H., 1940. Pleistocene mammals from the Ma Kai valley of northern Yunnan, China. *American Museum Novitates* 1009, 1–10.
- DeCelles, P.G., Quade, J., Kapp, P., Fan, M.J., Dettman, D.L., Ding, L., 2007. High and dry in central Tibet during the Late Oligocene. *Earth and Planetary Science Letters* 253, 389–401.
- deMenocal, P., Bloemendal, J., King, J., 1991. A rock-magnetic record of monsoonal dust deposition to the Arabian Sea: evidence for a shift in the mode of deposition at 2.4 Ma. *Proceedings of the Ocean Drilling Program, Scientific Results* 117, 389–407.
- Ding, Z.L., Yang, S.L., 2000. C_3/C_4 vegetation evolution over the last 7.0 Myr in the Chinese Loess Plateau: evidence from pedogenic carbonate $\delta^{13}C$. *Palaeogeography, Palaeoclimatology, Palaeoecology* 160, 291–299.
- Fang, X.M., Zhao, Z.J., Li, J.J., Yan, M.D., Pan, B.T., Song, C.H., Dai, S., 2005. Magnetostratigraphy of the late Cenozoic Laojunmiao anticline in the northern Qilian Mountains and its implications for the northern Tibetan Plateau uplift. *Science in China* 48, 1040–1051.
- Fang, X.M., Zhang, W.L., Meng, Q.Q., Gao, J.P., Wang, X.M., King, J., Song, C.H., Dai, S., Miao, Y.F., 2007. High-resolution magnetostratigraphy of the Neogene Huaitoutala section in the eastern Qaidam Basin on the NE Tibetan Plateau, Qinghai Province, China and its implication on tectonic uplift of the NE Tibetan Plateau. *Earth and Planetary Science Letters* 258, 293–306.
- Folk, R.L., Ward, W.C., 1957. Brazos River bar: A study in the significance of grain size parameters. *Journal of Sedimentary Petrology* 27, 3–26.
- Garzione, C.N., Dettman, D.L., Quade, J., DeCelles, P.G., Butler, R.F., 2000. High times on the Tibetan Plateau: paleoelevation of the Thakkhola graben, Nepal. *Geology* 28, 339–342.
- Gupta, A.K., Thomas, E., 2003. Initiation of Northern Hemisphere glaciation and strengthening of the northeast Indian monsoon: Ocean Drilling Program Site 758, eastern equatorial Indian Ocean. *Geology* 31, 47–50.
- Gupta, A.K., Singh, R.K., Joseph, S., Thomas, E., 2004. Indian Ocean high-productivity event (10–8 Ma): linked to global cooling or to the initiation of the Indian monsoons? *Geology* 32, 753–756.
- Hahn, D.G., Manabe, S., 1975. The role of mountains in the South Asian monsoon circulation. *Journal of the Atmospheric Sciences* 32, 1515–1541.
- Håkanson, L., Jansson, M., 1983. *Principles of Lake Sedimentology*. Springer, p. 316.
- Haug, G.H., Tiedemann, R., 1998. Effect of the formation of the Isthmus of Panama on Atlantic Ocean thermohaline circulation. *Nature* 393, 673–676.
- Hovan, S.A., Rea, D.K., 1992. The Cenozoic record of continental mineral deposition on Broken and Ninety east Ridges, Indian Ocean: Southern African aridity and sediment delivery from the Himalayas. *Paleoceanography* 7, 833–860.
- Hu, C.C., 1973. Ape–man teeth from Yuanmo, Yunnan. *Acta Geologica Sinica* 47, 65–71.
- Inman, D.L., 1949. Sorting of sediments in the light of fluid mechanics. *Journal of Sedimentary Petrology* 19, 51–70.
- Jiang, N.R., Sun, R., Liang, Q.Z., 1989. The Late Cenozoic Stratigraphy and Palaeontology in Yuanmo Basin, Yunnan, China. *Yunnan Geology (Supplement)*, Yunnan Institute of Geological Sciences, p. 108.
- Kleiven, H.F., Jansen, E., Fronval, T., Smith, T.M., 2002. Intensification of Northern Hemisphere glaciations in the circum Atlantic region (3.5–2.4 Ma) – ice-rafted detritus evidence. *Palaeogeography, Palaeoclimatology, Palaeoecology* 184, 213–223.
- Kroon, D., Steens, T., Troelstra, S.R., 1991. Onset of monsoonal related upwelling in the western Arabian Sea as revealed by planktonic foraminifers. *Proceedings of the Ocean Drilling Program, Scientific Results* 117, 257–263.
- Kutzbach, J.E., Prell, W.L., Ruddiman, W.F., 1993. Sensitivity of Eurasian climate to surface uplift of the Tibetan Plateau. *Journal of Geology* 101, 177–190.
- Li, J.J., 1995. Uplift of Qinghai–Xizang (Tibet) Plateau and Global Change. Lanzhou University Press, p. 207.
- Li, K., 1993. *Annals of Yuanmo County*. Yunnan People's Press, pp. 30–51.
- Li, P., Qian, F., Ma, X.H., Pu, Q.Y., Xing, L.S., Ju, S.Q., 1976. Preliminary study on the age of the fossil Yuanmo Man with a paleomagnetic method. *Science in China* 6, 579–591.
- Middleton, G.V., 1976. Hydraulic interpretation of sand size distributions. *Journal of Geology* 84, 405–426.
- Nie, J.S., King, J.W., Fang, X.M., 2008a. Link between benthic oxygen isotopes and magnetic susceptibility in the red-clay sequence on the Chinese Loess Plateau. *Geophysical Research Letters* 35, L03703. doi:10.1029/2007GL032817.
- Nie, J.S., King, J.W., Fang, X.M., 2008b. Tibetan uplift triggered the 400 k.y. signals in paleoclimatic records at 4 Ma. *Geological Society of America Bulletin* 120, 1338–1344.
- Prell, W.L., Kutzbach, J.E., 1992. Sensitivity of the Indian monsoon to forcing parameters and implications for its evolution. *Nature* 360, 647–652.
- Pye, K., 1987. *Aeolian Dust and Dust Deposits*. Academic Press, pp. 29–62.
- Qian, F., Pu, Q.Y., Wang, D.S., 1984. The discovery of the teeth of Yuanmo Man. In: Zhou, G.X., Zhang, X.Y. (Eds.), *Yuanmo Man*. Yunnan People's Press, pp. 3–7.
- Qian, F., Zhou, G.X., 1991. *Quaternary geology and palaeoanthropology of Yuanmo, Yunnan, China*. Science Press, New York, p. 222.
- Rea, D.K., Snoeckx, H., Joseph, L.H., 1998. Late Cenozoic eolian deposition in the North Pacific: Asia drying, Tibetan uplift, and cooling of the northern hemisphere. *Paleoceanography* 13, 215–224.
- Rowley, D.B., Currie, B.S., 2006. Palaeo-altimetry of the late Eocene to Miocene Lunpola basin, central Tibet. *Nature* 439, 677–681.
- Shackleton, N.J., Hall, M.A., Pate, D., 1995. Pliocene stable isotope stratigraphy of Site 846. *Proceedings of the Ocean Drilling Program, Scientific Results* 138, 337–355.
- Sly, P.G., 1978. Sedimentary processes in lakes. In: Lerman, A. (Ed.), *Lakes: Chemistry, Geology, Physics*. Springer, pp. 65–89.
- Sly, P.G., 1989a. Sediment dispersion: part 1, fine sediments and significance of the silt/clay ratio. *Hydrobiologia* 176 (177), 99–110.
- Sly, P.G., 1989b. Sediment dispersion: part 2, characterisation by size of sand fraction and per cent mud. *Hydrobiologia* 176 (177), 111–124.
- Spicer, R.A., Harris, N.B.W., Widdowson, M., Herman, A.B., Guo, S.X., Valdes, P.J., Wolfe, J.A., Kelley, S.P., 2003. Constant elevation of southern Tibet over the past 15 million years. *Nature* 421, 622–624.
- Sun, D.H., Bloemendal, J., Rea, D.K., Vandenberghe, J., Jiang, F.C., An, Z.S., Su, R.X., 2002. Grain-size distribution function of polymodal sediments in hydraulic and aeolian environments, and numerical partitioning of the sedimentary components. *Sedimentary Geology* 152, 263–277.
- Tanner, W.F., 1964. Modification of sediment size distributions. *Journal of Sedimentary Petrology* 34, 156–164.
- Urabe, A., Nakaya, H., Muto, T., Katoh, S., Hyodo, M., Xue, S.R., 2001. Lithostratigraphy and depositional history of the Late Cenozoic hominid-bearing successions in the Yuanmo Basin, southwest China. *Quaternary Science Reviews* 20, 1671–1681.
- Visher, G.S., 1969. Grain size distributions and depositional processes. *Journal of Sedimentary Petrology* 39, 1074–1106.
- Wang, H.J., 1999. Role of vegetation and soil in the Holocene megathermal climate over China. *Journal of Geophysical Research* 104, 9361–9367.
- Webster, P.J., 1987. The elementary monsoon. In: Fein, J.S., Stephens, P.L. (Eds.), *Monsoons*. John Wiley, pp. 3–32.
- Xiao, J.L., Chang, Z.G., Si, B., Qin, X.G., Itoh, S., Lomtatidze, Z., 2009. Partitioning of the grain-size components of Dali Lake core sediments: evidence for lake-level changes during the Holocene. *Journal of Paleolimnology*. doi:10.1007/s10933-008-9274-7.
- Yeh, T.C., Gao, Y.X., 1979. *Meteorology of the Tibetan Plateau*. Science Press, p. 258.
- Zachos, J., Pagani, M., Sloan, L., Thomas, E., Billups, K., 2001. Trends, rhythms, and aberrations in global climate 65 Ma to present. *Science* 292, 686–693.
- Zhang, Z.H., Liu, P.G., Qian, F., Min, L.R., Wang, Q., Zong, G.F., 1994. New development in research of late Cenozoic stratigraphy in Yuanmo Basin. *Marine Geology and Quaternary Geology* 14, 1–18.
- Zheng, H.B., Powell, C.M., An, Z.S., Zhou, J., Dong, G.R., 2000. Pliocene uplift of the northern Tibetan Plateau. *Geology* 28, 715–718.
- Zhu, R.X., Potts, R., Pan, Y.X., Lü, L.Q., Yao, H.T., Deng, C.L., Qin, H.F., 2008. Paleomagnetism of the Yuanmo Basin near the southeastern margin of the Tibetan Plateau and its constraints on late Neogene sedimentation and tectonic rotation. *Earth and Planetary Science Letters*. doi:10.1016/j.epsl.2008.04.016.